Digital Signal Processing 36 (2015) 144–155

Contents lists available at ScienceDirect

Digital Signal Processing

www.elsevier.com/locate/dsp

Information hiding with maximum likelihood detector for correlated signals

Sayed Mohammad Ebrahim Sahraeian [a], Mohammad Ali Akhaee [b,*], Bulent Sankur [c], Farokh Marvasti [d]

[a] Department of Electrical Engineering, University of California at Berkeley, CA 94720-3102, USA
[b] School of Electrical and Computer Engineering, College of Engineering, University of Tehran, Tehran, Iran
[c] Electrical and Electronic Engineering Department, Bogazici University, Bebek, 34342, Istanbul, Turkey
[d] Advanced Communication Research Institute (ACRI), Department of Electrical Engineering, Sharif University of Technology, Tehran, Iran

ARTICLE INFO

Article history:
Available online 2 October 2014

Keywords:
Maximum likelihood detector
Gaussian distribution
First-order autoregressive model
Information hiding
Scaling based rule

ABSTRACT

In this paper, a new scaling based information hiding approach with high robustness against noise and gain attack is presented. The host signal is assumed to be stationary Gaussian with first-order autoregressive model. For data embedding, the host signal is divided into two parts, and just one patch is manipulated while the other one is kept unchanged for parameter estimation. A maximum likelihood (ML) decoder is proposed which uses the ratio of samples for decoding the watermarked data. Due to the decorrelating property of the proposed decoder, it is very efficient for watermarking highly correlated signals for which the decoding process is not straightforward. By calculating the distribution of the decision variable, the performance of the decoder is analytically studied. To verify the validity of the proposed algorithm, it is applied to artificial Gaussian autoregressive signals. Simulation results for highly correlated host signals confirm the robustness of our decoder.

1. Introduction

Digital watermarking embeds information within a digital work so that the inserted data becomes part of its medium. This technique serves various purposes such as intellectual right protection, broadcast monitoring, data authentication, data indexing, and metadata insertion [1–4]. A digital watermarking system should successfully satisfy trade-offs between conflicting requirements of perceptual transparency, data capacity and robustness against attacks [5]. There exists a trade-off in satisfying these requirements. Depending on the application, the importance of each requirement varies. For example, for secret communication purposes, noise immunity and data rate are more important, while for data authentication, imperceptibly and robustness are more significant.

While increasing the strength of the watermark obviously provides higher resistance against attacks, more intelligent designs select image features that are relatively more immune. This has led to a number of algorithms that make watermark insertion dependent upon image content. This principle is implemented widely in multiplicative watermarking [6] and recently in a scaling-based [7] method. To effectively hide the information, these approaches often employ various transform domains such as Discrete Cosine Transform (DCT), Discrete Fourier Transform (DFT), and Discrete Wavelet Transform (DWT) [8–10], which concentrate the energy of the host signal in fewer components. Since correlation detection is suboptimal for multiplicative watermarking in the transform domain, several alternative optimum and locally optimum decoders have been proposed [6,11–16]. Cheng and Huang [11] proposed a robust optimum detector for the multiplicative rule in the DCT, DWT and DFT domains. In their algorithm, they modeled the distribution of high frequency coefficients of DCT and DWT as Generalized Gaussian while they assumed the magnitude of DFT coefficients to have Weibull distribution.

In most current approaches [6–8,12,14–16], the transform coefficients are assumed to be i.i.d. (independent identically distributed) for convenience while this is not necessarily true in all environments. In fact there are steganalysis systems that explicitly use the dependency of DCT and DWT coefficients at inter-block level or at intra-block level [17,18]. These authors model the dependence of transform coefficients with Markov chains. Furthermore, there are several studies that exploit the correlation of discrete trigonometric transform (DTT) coefficients for data compression [19,20,22]. For instance, the variance spectrum of the

* Corresponding author.
E-mail addresses: msahraeian@berkeley.edu (S.M.E. Sahraeian), akhaee@ut.ac.ir (M.A. Akhaee), bulent.sankur@boun.edu.tr (B. Sankur), marvasti@sharif.edu (F. Marvasti).

http://dx.doi.org/10.1016/j.dsp.2014.09.003
1051-2004/

DCT coefficients in sub-blocks of images is characterized with an autoregressive (AR) model in [20], or the 2-D block spectrum of natural images is estimated by 1-D AR model [21]. Recently, Hsu and Liu [22] showed that AR modeling can be considered for temporal/spectral envelope of DTT coefficients.

This paper brings two new contributions to the watermarking methodologies. First, we develop a blind method that is robust to local gain attacks, that is spatial modulation. If the watermarked samples are subjected to modifications with spatially varying gain, it is desirable that the data hiding scheme preserve its watermark after this attack. The proposed method to this effect is a generalization of the data hiding scheme [7], the multi-bit scaling-based method, to a blind scheme. The method in [7] assumes the existence of a side information channel, but in practice it may be difficult to guarantee any such secure channel. Second, our method does not assume the cover signal samples to be i.i.d or uncorrelated. We assume autoregressive model of order one (AR(1)) to represent the host signal, not only because it is a common model for images, but it also leads to a closed form solution in our watermarking system. Similar to the patchwork approach [23], we separate the host signal into two subsets. One of them is left intact and serves for parameter estimation at the decoder site. The terms of the other subset are watermarked with the so-called scaling-based watermarking, which uses slight amplification or attenuations depending on the watermark bit. The strength of the algorithm comes from the fact that it is the ratio of samples that carry the watermark information instead of sample values themselves. This makes the algorithm not only suitable for highly correlated signals but also invariant to gain attack. The method is studied analytically using exact derivations to the extent possible, and approximations are introduced when analysis becomes intractable.

The rest of the paper is organized as follows: Statistical models of the signals occurring in the embedding and decoding stages are presented in Section 2. In Section 3, the ratio-based watermarking method is introduced. Performance analysis of the proposed method is given in Section 4. Section 5 contains simulation results to investigate the robustness of the proposed approach against AWGN attack and performance comparisons vis-a-vis other watermarking techniques. Finally, Section 6 concludes the paper.

2. Signal modeling

In this section, we show certain statistical properties of the carrier signal relevant for our watermarking algorithm. We assume that the cover signal is first-order Gauss–Markov signal, it is highly correlated, but it has low coefficient of variation. For example, the approximation band of the wavelet decomposed images has this property as discussed in Appendix A, hence the signal model is not restrictive. We can obtain a closed form solution for this signal model, but otherwise our watermarking algorithm applies to other signals as well. However for the other signal models a close form decoder may not exist. It is worth mentioning that we assume zig–zag scanning in ordering the image coefficients throughout the paper.

Let, $\mathbf{u}$ be this Gauss–Markov host sequence with mean μ, variance σ^2, and correlation coefficient ρ. The N samples $u_1, u_2, ..., u_N$ of this parent sequence are split into two child sequences $\mathbf{x}$ and $\mathbf{y}$ consisting of the odd and even indexed terms, respectively: $x_i = u_{2i-1}$, $y_i = u_{2i}$, $i = 1, 2, ..., \frac{N}{2}$. These $\mathbf{x}$ and $\mathbf{y}$ are also Gauss–Markov subsequences with means and variances identical to those of their parent, that is, with $x = \mathcal{N}(\mu_x, \sigma_x^2)$ and $y = \mathcal{N}(\mu_y, \sigma_y^2)$. Their auto-correlation coefficients are ρ^2 and their cross-correlation coefficient is ρ.

The carrier signal, $\mathbf{z}$, is another sequence formed as the term-wise ratio of the two subsequences. The ratio sequence, as discussed in Section 3.2, will be used to build our optimum watermarking decoder.

We construct the ratio sequence $\mathbf{z}$ as follows:

$$z_i = \frac{x_i}{y_i} = \frac{u_{2i-1}}{u_{2i}}, \quad i = 1, ..., \frac{N}{2}. \tag{1}$$

The probability density function of z for $\mu_y \neq 0$ is given as [25]:

$$f(z) = \frac{b(z)d(z)}{\sqrt{2\pi}\sigma_x\sigma_y a^3(z)}\left[2\Phi\left\{\frac{b(z)}{ra(z)}\right\} - 1\right] + \frac{re^{-c/2r^2}}{\pi\sigma_x\sigma_y a^2(z)} \tag{2}$$

where,

$$a(z) = \sqrt{\frac{z^2}{\sigma_x^2} - \frac{2\rho z}{\sigma_x\sigma_y} + \frac{1}{\sigma_y^2}},$$

$$b(z) = \frac{\mu_x z}{\sigma_x^2} - \frac{\rho(\mu_x + \mu_y z)}{\sigma_x\sigma_y} + \frac{\mu_y}{\sigma_y^2},$$

$$c = \frac{\mu_x^2}{\sigma_x^2} - \frac{2\rho\mu_x\mu_y}{\sigma_x\sigma_y} + \frac{\mu_y^2}{\sigma_y^2},$$

$$d(z) = \exp\left\{\frac{b^2(z) - ca^2(z)}{2r^2a^2(z)}\right\},$$

$r = 1 - \rho^2$, and $\Phi(t) = \int_{-\infty}^{t} \frac{1}{\sqrt{2\pi}} e^{-\frac{1}{2}r^2}\, dr$. In the special case of zero-mean variates, that is for $\mu_x = \mu_y = 0$, the distribution becomes Cauchy [24].

As we will see here, for the case of non zero μ_x and μ_y, and $\sigma_y \ll \mu_y$, $\sigma_x \ll \mu_x$, the distribution of $z = \frac{x}{y}$ can be well approximated by a Gaussian distribution. As shown in Appendix A, these small variance-to-mean conditions occur easily in the approximation bands of the wavelet decomposition of images. The parameters μ_z and σ_z^2 of the Gaussian approximation can be computed as follows. If we define $\bar{x} = x - \mu_x$, $\bar{y} = y - \mu_y$, and $\bar{z} = z - \mu_z$, we have:

$$\begin{aligned}\mu_z + \bar{z} = \frac{\mu_x + \bar{x}}{\mu_y + \bar{y}} &= \frac{\mu_x(1 + \frac{\bar{x}}{\mu_x})}{\mu_y(1 + \frac{\bar{y}}{\mu_y})} \simeq \frac{\mu_x}{\mu_y}\left(1 + \frac{\bar{x}}{\mu_x}\right)\left(1 - \frac{\bar{y}}{\mu_y}\right) \\ &\simeq \frac{\mu_x}{\mu_y}\left(1 + \frac{\bar{x}}{\mu_x} - \frac{\bar{y}}{\mu_y} - \frac{\bar{x}\bar{y}}{\mu_x\mu_y}\right).\end{aligned} \tag{3}$$

Taking the expectation of both sides of (3) and considering the fact that As $E(\bar{x}) = E(\bar{y}) = E(\bar{z}) = 0$, and $E(\bar{x}\bar{y}) = E((x-\mu_x)(y-\mu_y)) = \rho\sigma_x\sigma_y$, we have:

$$\mu_z = \frac{\mu_x}{\mu_y} \cdot E\left(1 + \frac{\bar{x}}{\mu_x} - \frac{\bar{y}}{\mu_y} - \frac{\bar{x}\bar{y}}{\mu_x\mu_y}\right) = \frac{\mu_x}{\mu_y} - \frac{\rho\sigma_x\sigma_y}{\mu_y^2} \tag{4}$$

Subtracting (3) from (4), we have:

$$\bar{z} = \frac{\mu_x}{\mu_y}\left(\frac{\bar{x}}{\mu_x} - \frac{\bar{y}}{\mu_y} - \frac{\bar{x}\bar{y}}{\mu_x\mu_y}\right) + \frac{\rho\sigma_x\sigma_y}{\mu_y^2} \tag{5}$$

Thus:

$$\begin{aligned}\sigma_z^2 = E(\bar{z}^2) = E\Bigg[&\left(\frac{\bar{x}}{\mu_y}\right)^2 + \left(\frac{\mu_x\bar{y}}{\mu_y^2}\right)^2 + \left(\frac{\bar{x}\bar{y}}{\mu_y^2}\right)^2 \\ &+ \frac{\rho^2\sigma_x^2\sigma_y^2}{\mu_y^4} - 2\frac{\mu_x\bar{x}\bar{y}}{\mu_y^3} - 2\frac{\bar{x}^2\bar{y}}{\mu_y^3} + 2\frac{\mu_x\rho\sigma_x\sigma_y\bar{x}}{\mu_y^3} \\ &+ 2\frac{\mu_x\bar{x}\bar{y}^2}{\mu_y^4} - 2\frac{\mu_x\bar{y}\sigma_x\sigma_y}{\mu_y^4} - 2\frac{\rho\sigma_x\sigma_y\bar{x}\bar{y}}{\mu_y^4}\Bigg]\end{aligned} \tag{6}$$

Now, to compute $E(\bar{x}^2\bar{y})$ consider that we write $\bar{y}$ as $\bar{y} = r_1\bar{x} + r_2$ where r_1 represents the correlated part of $\bar{y}$ and r_2 represents the

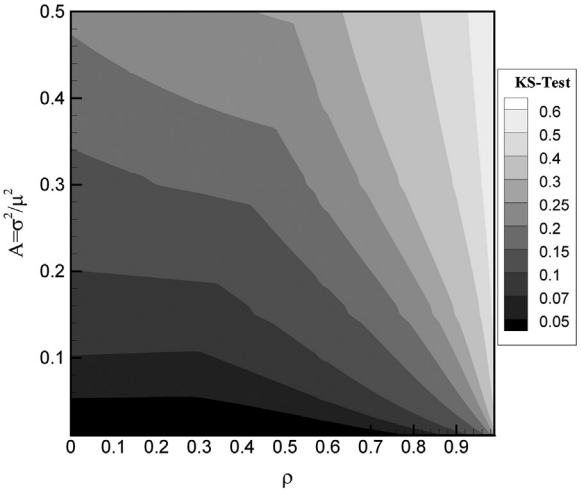

Fig. 1. The Kolmogorov–Smirnov distance between the proposed Gaussian approximation distribution and Hinkley's distribution for different coefficient of variation, A and normalized correlation coefficient ρ.

uncorrelated part of $\bar{y}$. Thus we have $E(\bar{x}^2\bar{y}) = r_1 E(\bar{x}^3) + 0$, and as we have considered the zero skewness, we have $E(\bar{x}^2\bar{y}) = 0$. In a same way, we can show that $E(\bar{x}\bar{y}^2) = 0$. Besides using the four Gaussian formula [24], we can show that $E(\bar{x}^2\bar{y}^2) = \sigma_x^2\sigma_y^2(1 + 2\rho^2)$. Therefore, (6) is converted to:

$$\sigma_z^2 = \frac{\sigma_x^2}{\mu_y^2} + \frac{\mu_x^2\sigma_y^2}{\mu_y^4} + \frac{\sigma_x^2\sigma_y^2(1+\rho^2)}{\mu_y^4} - 2\frac{\mu_x\rho\sigma_x\sigma_y}{\mu_y^3} \tag{7}$$

Now we invoke the fact that the parent sequence u is stationary, thus, the samples of the subsequences must have $\sigma_x \simeq \sigma_y \simeq \sigma$ and $\mu_x \simeq \mu_y \simeq \mu$. As a consequence, μ_z and σ_z can be computed as:

$$\mu_z = 1 - \rho\frac{\sigma^2}{\mu^2} = 1 - \rho A \tag{8}$$

$$\sigma_z^2 = (2 - 2\rho)A + \left(1 + \rho^2\right)A^2 \tag{9}$$

where $A = \frac{\sigma^2}{\mu^2}$. Here A can be interpreted as squared coefficient of variation.

In Fig. 1, the Kolmogorov–Smirnov test (KS-test), that is $\sup|F_1(z) - F_2(z)|$, between the Gaussian approximation with parameters in (8) and (9) and Hinkley's distribution (2) for different values of the coefficient of variation, A and of the correlation coefficient ρ is shown. As we can see for wide parameter range of $\rho \in [0, 0.9]$ and $A \in [0, 0.4]$ the Gaussian approximation to Hinkley's distribution holds within a Kolmogorov–Smirnov distance of less than 0.2. In a practical case, we show that for the approximation band of the wavelet decomposition we have $A < 0.1$ and $\rho \in [0.2, 0.7]$ which correspond to KS distances less than 0.07 (see Appendix A).

To find the correlation coefficients between the z_i sample, considering the first order Markov chain for $\mathbf{u}$ sequence, we have:

$$\begin{aligned} E(z_i z_{i+1}) &= E\left(\frac{x_i}{y_i}\cdot\frac{x_{i+1}}{y_{i+1}}\right) = E\left(\frac{\mu+\bar{u}_{2i-1}}{\mu+\bar{u}_{2i}}\cdot\frac{\mu+\bar{u}_{2i+1}}{\mu+\bar{u}_{2i+2}}\right) \\ &\simeq E\left\{\left(1+\frac{\bar{u}_{2i-1}}{\mu}\right)\left(1-\frac{\bar{u}_{2i}}{\mu}\right)\left(1+\frac{\bar{u}_{2i+1}}{\mu}\right)\right. \\ &\quad \left.\times\left(1-\frac{\bar{u}_{2i+2}}{\mu}\right)\right\} \end{aligned} \tag{10}$$

Considering the fact that $E(\bar{u}_i) = 0$, $E(\bar{u}_i\bar{u}_j\bar{u}_k) = 0$, $E(\bar{u}_i\bar{u}_j) = \sigma^2\rho^{|i-j|}$, and $E(\bar{u}_i\bar{u}_{i+1}\bar{u}_{i+2}\bar{u}_{i+3}) = \sigma^4(\rho^2 + 2\rho^4)$, (10) converts to:

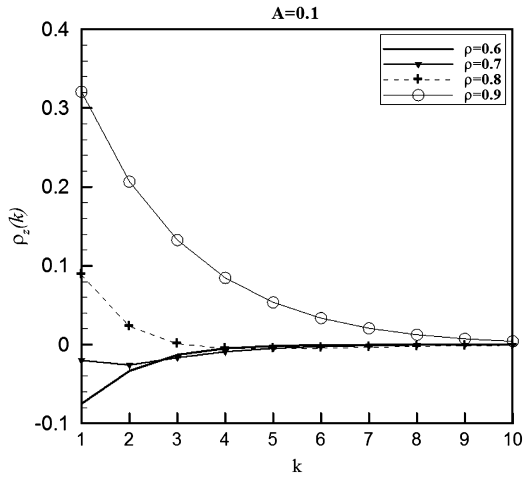

Fig. 2. The speed of decay of the correlation coefficient $\rho_z(k)$ as a function of the lag k for $A = 0.1$ and ρ in [0.6–0.9].

$$E(z_i z_{i+1}) = 1 - \left(\rho^3 - 2\rho^2 + 3\rho\right)\frac{\sigma^2}{\mu^2} + \left(\rho^2 + 2\rho^4\right)\frac{\sigma^4}{\mu^4} \tag{11}$$

Using (9) and (11) the correlation coefficient at lag 1, is calculated as follows:

$$\rho_z(1) = \frac{E(z_i z_{i+1}) - \mu_z^2}{\sigma_z^2} = \frac{2\rho^4 A - (\rho^3 - 2\rho^2 + \rho)}{(1+\rho^2)A + (2 - 2\rho)} \tag{12}$$

Notice that for all A, one has $\lim_{\rho\to 0}\rho_z(1) = 0$, and for values that A is not near zero $\lim_{\rho\to 1}\rho_z(1) = 1$. For $A \ll 1$ one has $\rho_z(1) \simeq \frac{1}{2}\rho(\rho - 1)$.

We can similarly compute correlation coefficients at higher lags as:

$$\rho_z(k) = \frac{E(z_i z_{i+k}) - \mu_z^2}{\sigma_z^2} = \frac{2\rho^{4k}A - \rho^{2k-1}(\rho-1)^2}{(1+\rho^2)A + (2-2\rho)} \tag{13}$$

Fig. 2 depicts the speed of decay of the correlation coefficient $\rho_z(k)$ as a function of the lag k for $A = 0.1$ and ρ in [0.6–0.9].

The approximation to the Hinkley density function $f(\mathbf{z})$ for a vector $\mathbf{z} = \{z_1, z_2, \cdots, z_{\frac{N}{2}}\}$ observation is given as:

$$f(\mathbf{z}) = \frac{1}{\sqrt{(2\pi)^{\frac{N}{2}}|\mathbf{C}|^{\frac{1}{2}}}} e^{-\frac{1}{2}[(\mathbf{z}-\mu_z)^T\mathbf{C}^{-1}(\mathbf{z}-\mu_z)]} \tag{14}$$

where the element c_{ih} of the covariance matrix $\mathbf{C} = \{c_{ih}\}$ is computed as $E(z_i z_h) - \mu_z^2 = \rho_z(|i-h|)\sigma_z^2$.

For the signals of interest, i.e., sequences with a small coefficient of variation ($A \ll 1$), we can approximate the correlation coefficients as $\rho_z(k) \simeq \rho^{(2k-2)}\rho_z(1)$ (see also Appendix A), so that an element of $\mathbf{C}$ can be expressed as $c_{ih} \simeq \rho^{2|i-h|-2}\rho_z(1)$ for $i \neq h$. Thus, we can approximate $\mathbf{C}$ as follows (for simplicity we show $\rho_z(1)$ as ρ_z from now on):

$$\mathbf{C} \simeq \sigma_z^2\begin{bmatrix} 1 & \rho_z & \rho^2\rho_z & \rho^4\rho_z & \cdots \\ \rho_z & 1 & \rho_z & \rho^2\rho_z & \cdots \\ \rho^2\rho_z & \rho_z & 1 & \rho_z & \cdots \\ \rho^4\rho_z & \rho^2\rho_z & \rho_z & 1 & \cdots \\ \cdots & \cdots & \cdots & \cdots & \cdots \end{bmatrix}. \tag{15}$$

Note that the $A \ll 1$ condition allows us to approximate the correlation coefficient of the z ratio sequence as $\rho_z \simeq \frac{1}{2}\rho(\rho - 1)$. We notice that the z sequence will have low correlation values not only for the obvious case of low-correlated parent sequence $\mathbf{u}$ (i.e., $\rho \ll 1$), but even for highly correlated $\mathbf{u}$ sequences (ρ is near

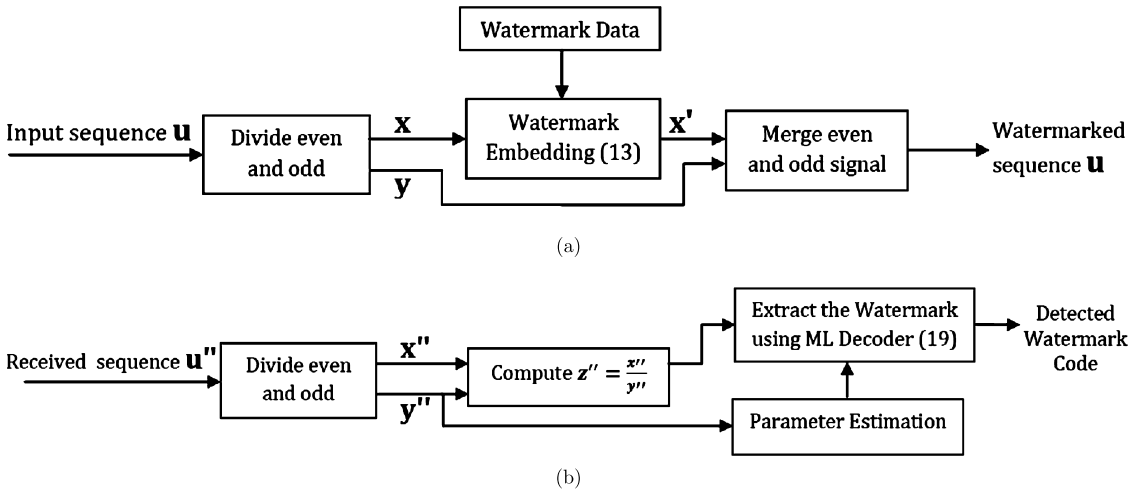

Fig. 3. The block diagram of the proposed watermarking method (a) embedding, (b) decoding.

unity) when $A \ll 1$ condition is satisfied. For example, we computed the A, ρ, and ρ_z parameters of 1000 test images. We found that their mean values were respectively, $A = 0.02$, $\rho = 0.45$, and $\rho_z = 0.12$ for the Level II wavelet approximation coefficients (see for more detailed plots Appendix A).

We will exploit this characteristics for watermark detection.

In any case, since ρ_z is always quite smaller than ρ, we can model $\mathbf{z}$ as a first-order Markov sequence and approximate the joint density of the $N/2$ long sequence as:

$$f(\mathbf{z}) \simeq f(z_1) f(z_2|z_1) \cdots f(z_{\frac{N}{2}}|z_{\frac{N}{2}-1}) \tag{16}$$

Furthermore, the z_i behave as if they were jointly Gaussian, hence we have:

$$f(z_2|z_1) = \frac{1}{\sqrt{2\pi(1-\rho_z^2)\sigma_z^2}} \exp\left\{-\frac{(\bar{z}_2 - \rho_z \bar{z}_1)^2}{2(1-\rho_z^2)\sigma_z^2}\right\} \tag{17}$$

where, $\bar{z}_i = z_i - \mu_z$ are the centered variates. As shown in Appendix B, for $\rho_z \ll 1$ and with some simplification in (17), we can rewrite (16) as:

$$f(\mathbf{z}) \simeq \frac{e^{-\frac{1}{2\sigma_z^2}\sum_1^{\frac{N}{2}} \bar{z}_i^2}}{\sqrt{(2\pi\sigma_z^2)^{\frac{N}{2}}}} \left[1 + \frac{\rho_z}{\sigma_z^2} \sum_{i=2}^{\frac{N}{2}} (\bar{z}_i \bar{z}_{i-1})\right] \tag{18}$$

3. Proposed watermarking method

In the sequel, we introduce our blind watermarking algorithm based on the signal model in Section 2 and derive its Maximum Likelihood (ML) detection. The blindness of the algorithm hinges on the strategy of using two companion subsequences, one for signal embedding and one as a reference to estimate the decoder parameters. To clarify the notation, we remark that unprimed quantities such as x, y or u denote the source sequences; the primed quantities x' or u' denote the watermarked sequences (note the absence of y' since the even sequence is left intact), and finally double-primed quantities x'', y'' or u'' denote the noisy (attacked) versions of the sequences at the receiver.

The block diagram of the proposed watermarking method is shown in Fig. 3 and the embedding and decoding strategies are summarized in Table 1.

3.1. Watermark embedding

As increasing the watermarking strength improves robustness, intelligent designs make the watermark insertion dependent upon the host signal content. One of the well-known methods to realize this fact is through multiplicative watermarking rules. Among multiplicative rules, here we adopt up-and-down scaling scheme proposed in [7]. In this technique the host sequence does not produce high frequency artifacts on the watermarked signal.

Table 1
Proposed embedding and decoding strategies.

Embedding	$x'_i = \begin{cases} x_i \cdot \alpha & \text{for embedding 1} \\ x_i \cdot \frac{1}{\alpha} & \text{for embedding } -1 \end{cases}$
Decoding G-ORD	$f(\mathbf{z}''\|1) \gtrless_{-1}^{1} f(\mathbf{z}''\|-1)$ with given in (27)
Decoding M-ORD	$f(\mathbf{z}''\|1) \gtrless_{-1}^{1} f(\mathbf{z}''\|-1)$ with $f(\mathbf{z}''\|\delta)$ given in (37)

In the scaling based watermarking approach, watermark embedding is based on the up-down scaling of the host sequence according to the message bit. Thus, the subsequence bearing the watermark code $\mathbf{x}$ is modulated as:

$$x'_i = \begin{cases} x_i \cdot \alpha & \text{for embedding 1} \\ x_i \cdot \frac{1}{\alpha} & \text{for embedding } -1 \end{cases} \tag{19}$$

where $\alpha > 1$ is some strength factor. Using this scaling-based rule in the time/spatial, frequency, or the wavelet transform domain, will produce minor artifact to the host signal (see Appendix A); thus, it preserves shape of the signal. The watermarked sequence, $\mathbf{u}'$ is constituted of the watermark-bearing part $\mathbf{x}'$ and of the intact reference part $\mathbf{y}$. Recall that these terms, correspond respectively to the odd and even indexed terms of $\mathbf{u}'$.

3.2. Watermark decoding

At the decoder site, we have the sequence $\mathbf{u}'' = \mathbf{u}' + \mathbf{n}'$, which is transmitted sequence $\mathbf{u}'$ contaminated by $\mathbf{n}'$, zero-mean Additive White Gaussian Noise (AWGN), $\mathbf{n}' \sim \mathcal{N}(0, \sigma_n^2)$. (We use the notation $\mathbf{n}'$ to mark the fact that channel noise contaminates the watermarked signal indicated by primed variables.) The decoder splits the received data into odd- and even-indexed subsequences. To simplify the notation, let us denote the odd- and even-indexed noise terms respectively as $n'_{x_i} = n'_{2i-1}$ and $n'_{y_i} = n'_{2i}$. The reference sequence in the receiver $y''_i = y_i + n'_{y_i}$, has the distribution of $\mathcal{N}(\mu, \sigma^2 + \sigma_n^2)$.

The distribution of the watermark bearing part, $x''_i = x'_i + n'_{x_i}$ for embedding the bit value $\delta \in \{-1, 1\}$ can be written as:

$$x''_{i|\delta} = x'_i + n'_{x_i} = \alpha^\delta \cdot x_i + n'_{x_i} \quad \Longrightarrow \quad x''_{i|\delta} \sim \mathcal{N}\left(\alpha^\delta \mu, \sigma^2_{x''_{|\delta}}\right) \tag{20}$$

where $\sigma^2_{x''_{|\delta}} = \alpha^{2\delta}\sigma^2 + \sigma_n^2$.

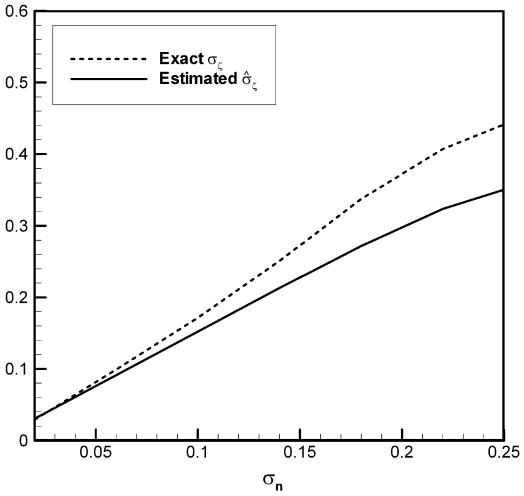

Fig. 4. Comparing the exact and the estimated variance of the residue term in z'' for different noise levels.

If we revert to the ratio sequence, that is, the ratio of "watermarked and noisy odd-indexed terms" to "not-watermarked but noisy even-indexed terms", $\mathbf{z}''$ becomes:

$$z''_i = \frac{x'_i + n'_{x_i}}{y_i + n'_{y_i}}, \quad i = 1, \cdots, \frac{N}{2}. \tag{21}$$

3.2.1. Noise term estimation

Since z''_i results from the ratio of two non-zero-mean Gaussian variables, its distribution for small amounts of noise can be estimated with the Gaussian approximation in Section 2. For instance, for the case of '1' embedding we have $x'_i = \alpha x_i$; thus, z''_i is the ratio of two Gaussian random variables $\mathcal{N}(\alpha\mu, \alpha^2\sigma^2 + \sigma_n^2)$ and $\mathcal{N}(\mu, \sigma^2 + \sigma_n^2)$. Besides, the correlation coefficient between the numerator and denominator of z''_i can be computed as:

$$\frac{E((x'_i + n'_{x_i})(y_i + n'_{y_i})) - \alpha\mu^2}{\sqrt{(\alpha^2\sigma^2 + \sigma_n^2)(\sigma^2 + \sigma_n^2)}} = \frac{\alpha\rho\sigma^2}{\sqrt{(\alpha^2\sigma^2 + \sigma_n^2)(\sigma^2 + \sigma_n^2)}}, \tag{22}$$

where we have used the whiteness of the noise sequence. Here, we can estimate the noise standard deviation σ_n from the HH1 wavelet subband, the diagonal subband in the first level of decomposition, by the robust median estimator, suggested in [26].

Thus, we can estimate the mean and variance of z''_i using (4), (6), (8), and (9) as:

$$\mu_{z''_i|1} = \alpha - \alpha\rho\frac{\sigma^2}{\mu^2} = \alpha\mu_z, \tag{23}$$

$$\sigma^2_{z''_i|1} = \alpha^2\sigma_z^2 + \frac{\sigma_n^2}{\mu^2}(1+\alpha^2)(1+A) + \frac{\sigma_n^4}{\mu^4} \tag{24}$$

Therefore, if we write $z''_{i|1} = z'_{i|1} + \zeta_{|1}$, where $z'_{i|1} = \frac{x'_i}{y_i} = \frac{\alpha x_i}{y_i}$ is the watermark signal term and $\zeta_{|1}$ is the residue term, knowing that $z'_{i|1} \sim \mathcal{N}(\alpha\mu_z, \alpha^2\sigma_z^2)$, from (23) and (24), (by independence assumption) we can approximate $\zeta_{|1}$ as a Gaussian residue term. Thus for $\delta \in \{-1, 1\}$ embedding, this Gaussian term will have the following parameters:

$$\mu_{\zeta|\delta} = 0, \qquad \sigma^2_{\zeta|\delta} = \frac{\sigma_n^2}{\mu^2}(1+\alpha^{2\delta})(1+A) + \frac{\sigma_n^4}{\mu^4}. \tag{25}$$

In summary, we extract the portions of (23) and (24) accounting the presence of the additive channel noises n'_x and n'_y. We will employ this ζ statistic in the analysis of the ML decoder.

In Fig. 4 we compare the exact and the estimated variances of the residue term in z'', i.e., ζ, for different additive noise levels. The host signal parameters are set at $\mu = 1$, $\sigma = 0.2$, and $\rho = 0.9$. The true variance, σ_ζ, and our estimate in (25) match well for $\sigma_n < 0.08$, which in fact corresponds to SNR > 22 dB. Notice that noise contamination below 22 dB SNR would invalidate the carrier signal itself. For the higher noise levels we can use function fitting to reduce the gap between the analytical and estimated noise terms.

3.2.2. Maximum likelihood decoder

The ML decoder using (14) becomes:

$$f(\mathbf{z}''|1) \gtrless_{-1}^{1} f(\mathbf{z}''|-1) \tag{26}$$

where $f(\mathbf{z}''|\delta)$ is given as:

$$f(\mathbf{z}''|\delta) = \frac{1}{\sqrt{(2\pi)^{\frac{N}{2}}|\mathbf{C}_{|\delta}|^{\frac{1}{2}}}} e^{-\frac{1}{2}[(\mathbf{z}''-\mu_{\mathbf{z}''_{|\delta}})^T \mathbf{C}_{|\mathbf{1}}{}^{-1}(\mathbf{z}''-\mu_{\mathbf{z}''_{|\delta}})]} \tag{27}$$

The covariance matrix for $\delta \in \{-1, 1\}$ embedding becomes: $\mathbf{C}_{|\delta} = \{c_{ih_{|\delta}}\}$ and

$$\begin{aligned} c_{ih_{|\delta}} &= E(z''_i z''_h) - \mu^2_{z''} = E\big[(z'_i + \zeta_{i|\delta})(z'_h + \zeta_{h|\delta})\big] - \mu^2_{z'} \\ &= E(z'_i z'_h) + E(\zeta_{i|\delta}\zeta_{h|\delta}) - \mu^2_{z'} \end{aligned} \tag{28}$$

and since $z'_i = \frac{x'_i}{y_i} = \alpha^\delta \frac{x_i}{y_i} = \alpha^\delta z_i$ for δ embedding, we have:

$$\begin{aligned} c_{ih_{|\delta}} &= \alpha^{2\delta} E(z_i z_h) + E(\zeta_{i|\delta}\zeta_{h|\delta}) - \alpha^{2\delta}\mu_z^2 \\ &= \alpha^{2\delta} c_{ih} + E(\zeta_{i|\delta}\zeta_{h|\delta}) \end{aligned} \tag{29}$$

Thus:

$$\mathbf{C}_{|\delta} = \alpha^{2\delta}\mathbf{C} + \sigma^2_{\zeta|\delta}\mathbf{I} \tag{30}$$

where $\mathbf{C}$ is given in (15). By substituting (27) in (26), we have:

$$\begin{aligned} &|\mathbf{C}_{|\mathbf{1}}|^{\frac{-1}{2}} e^{-\frac{1}{2}[(\mathbf{z}''-\mu_{\mathbf{z}''_{|\mathbf{1}}})^T \mathbf{C}_{|\mathbf{1}}{}^{-1}(\mathbf{z}''-\mu_{\mathbf{z}''_{|\mathbf{1}}})]} \\ &\quad \gtrless_{-1}^{1} |\mathbf{C}_{|-\mathbf{1}}|^{\frac{-1}{2}} e^{-\frac{1}{2}[(\mathbf{z}''-\mu_{\mathbf{z}''_{|-\mathbf{1}}})^T \mathbf{C}_{|-\mathbf{1}}{}^{-1}(\mathbf{z}''-\mu_{\mathbf{z}''_{|-\mathbf{1}}})]} \end{aligned} \tag{31}$$

We take the logarithm of both sides and simplify the result considering the symmetry of the $\mathbf{C}_{|\mathbf{1}}$ and $\mathbf{C}_{|-\mathbf{1}}$ matrices to obtain:

$$\begin{aligned} &\mathbf{z}''^T(\mathbf{C}_{|-\mathbf{1}}{}^{-1} - \mathbf{C}_{|\mathbf{1}}{}^{-1})\mathbf{z}'' \\ &\quad - 2\mathbf{z}''^T(\mathbf{C}_{|-\mathbf{1}}{}^{-1}\mu_{\mathbf{z}''_{|-\mathbf{1}}} - \mathbf{C}_{|\mathbf{1}}{}^{-1}\mu_{\mathbf{z}''_{|\mathbf{1}}}) \gtrless_{-1}^{1} T_1 \end{aligned} \tag{32}$$

where

$$T_1 = \log\frac{|\mathbf{C}_{|\mathbf{1}}|}{|\mathbf{C}_{|-\mathbf{1}}|} + \mu_{\mathbf{z}''_{|\mathbf{1}}}{}^T \mathbf{C}_{|\mathbf{1}}{}^{-1}\mu_{\mathbf{z}''_{|\mathbf{1}}} - \mu_{\mathbf{z}''_{|-\mathbf{1}}}{}^T \mathbf{C}_{|-\mathbf{1}}{}^{-1}\mu_{\mathbf{z}''_{|-\mathbf{1}}}$$

Notice that $\mu_{\mathbf{z}''_{|\mathbf{1}}}$ and $\mu_{\mathbf{z}''_{|-\mathbf{1}}}$ are $\frac{N}{2} \times 1$ size vectors with all components equal to $\alpha\mu_z$ and $\frac{\mu_z}{\alpha}$, respectively.

Thus, the ML watermark decoder depends parametrically upon μ_z, $\mathbf{C}_{|\mathbf{1}}$, and $\mathbf{C}_{|-\mathbf{1}}$ which in turn are functions of the host signal parameters ρ, μ and σ (the latter two take place in A), as well of the AWGN variance via $\sigma_{\zeta|1}$. If these parameters were to be set or communicated by the user, the algorithm would have been semi-blind. However, we can estimate μ, σ, and ρ parameters from the reference signal $y''_i = y_i + n'_{y_i}$, and hence the proposed algorithm qualifies as fully blind. We have the following estimates:

$$\hat{\mu} = \mu_{y''}, \qquad \hat{\sigma} = \sqrt{\max(\sigma^2_{y''} - \sigma_n^2, 0)},$$

$$\hat{\rho} = \sqrt{\rho_{y''}\frac{\hat{\sigma}^2 + \sigma_n^2}{\hat{\sigma}^2}} \tag{33}$$

Here, we have used the Markov model assumption for $\mathbf{u}$, to estimate ρ from $\rho_{y''}$, the latter being the correlation coefficient of $\mathbf{y}''$, and the formula reads as:

$$\rho_{y''} = \frac{E[(u_{2i}+n_{2i})(u_{2i+2}+n_{2i+2})]-\mu^2}{\sigma^2+\sigma_n^2} = \frac{E(u_{2i}u_{2i+2})-\mu^2}{\sigma^2+\sigma_n^2} = \rho^2\frac{\sigma^2}{\sigma^2+\sigma_n^2} \tag{34}$$

Further simplifications are in order for the ML decoder in (32) that avoid the inversion process of the two covariance matrices. Consider simpler realization of the two conditional densities in (18). For $\rho_z \ll 1$, we are able to simplify the densities of $\mathbf{z}''$ as:

$$f(\mathbf{z}'') \simeq \frac{e^{-\frac{1}{2\sigma_{z''}^2}\sum_1^{\frac{N}{2}}\bar{z}_i''^2}}{\sqrt{(2\pi\sigma_{z''}^2)^{\frac{N}{2}}}}\left[1+\frac{\rho_{z''}}{\sigma_{z''}^2}\sum_{i=2}^{\frac{N}{2}}(\bar{z}_i''\bar{z}_{i-1}'')\right] \tag{35}$$

where $\bar{z}_i'' = z_i'' - \mu_z'$, $\sigma_{z''}^2 = \sigma_{z'}^2+\sigma_\zeta^2$,

$$\rho_{z''} = \frac{E(z_i''z_{i+1}'')-\mu_{z''}^2}{\sigma_{z''}^2} = \frac{E(z_i'z_{i+1}')+E(\zeta_i\zeta_{i+1})-\mu_{z'}^2}{\sigma_{z''}^2} = \frac{E(z_i'z_{i+1}')-\mu_{z'}^2}{\sigma_{z''}^2} = \rho_{z'}\frac{\sigma_{z'}^2}{\sigma_{z''}^2} = \rho_z\frac{\sigma_{z'}^2}{\sigma_{z'}^2+\sigma_\zeta^2} \tag{36}$$

Adopting this approximation in the ML decision strategy in (26) the density function $f(\mathbf{z}''|\delta)$ for $\delta\in\{-1,1\}$ embedding will be:

$$f(\mathbf{z}''|\delta) \simeq \frac{1}{\sqrt{[2\pi(\alpha^{2\delta}\sigma_z^2+\sigma_{\zeta|\delta}^2)]^{\frac{N}{2}}}}\exp\left\{-\frac{\sum_1^{\frac{N}{2}}(z_i''-\alpha^\delta\mu_z)^2}{2(\alpha^{2\delta}\sigma_z^2+\sigma_{\zeta|\delta}^2)}\right\} \times\left[1+\frac{\alpha^{2\delta}\rho_z\sigma_z^2}{(\alpha^{2\delta}\sigma_z^2+\sigma_{\zeta|\delta}^2)^2} \times\sum_{i=2}^{\frac{N}{2}}\left[(z_i''-\alpha^\delta\mu_z)(z_{i-1}''-\alpha^\delta\mu_z)\right]\right] \tag{37}$$

Substituting (37) in the ML decision rule (26), taking the logarithm of both sides, and apply some simplifications, we have:

$$\left\{-\frac{N}{2}\log\frac{\sigma_{z''|1}^2}{\sigma_{z''|-1}^2}+(\sigma_{z''|-1}^{-2}-\sigma_{z''|1}^{-2})\sum_{i=1}^{\frac{N}{2}}z_i''^2 -2\mu_z\left(\frac{\alpha^{-1}}{\sigma_{z''|-1}^2}-\frac{\alpha}{\sigma_{z''|1}^2}\right)\sum_{i=1}^{\frac{N}{2}}z_i''+\frac{N}{2}\mu_z^2\left(\frac{\alpha^{-2}}{\sigma_{z''|-1}^2}-\frac{\alpha^2}{\sigma_{z''|1}^2}\right)\right\} \gtrless_{-1}^{1} 2\sum_{i=2}^{\frac{N}{2}}\log\left[\frac{1+\sigma_{z''|-1}^{-4}\alpha^{-2}\rho_z\sigma_z^2(z_i''-\frac{\mu_z}{\alpha})(z_{i-1}''-\frac{\mu_z}{\alpha})}{1+\sigma_{z''|1}^{-4}\alpha^2\rho_z\sigma_z^2(z_i''-\alpha\mu_z)(z_{i-1}''-\alpha\mu_z)}\right] \tag{38}$$

where $\sigma_{z''|1}^2 = \alpha^2\sigma_z^2+\sigma_{\zeta|1}^2$ and $\sigma_{z''|-1}^2 = \alpha^{-2}\sigma_z^2+\sigma_{\zeta|-1}^2$. As already remarked, μ_z, σ_z, and ρ_z are needed for watermark detection, which in turn depend on the host signal parameters μ, σ, and ρ. As discussed before, these parameters can be estimated from the received signal using (33).

In summary, the ML detector is based on the ratio of the interleaved samples of the received signal. We will call this detector as Optimum Ratio Decoding (ORD). If we implement it using (32), then we will call it Gaussian ORD (G-ORD) since the only assumption in (32) is the Gaussian modeling of the host signal as in (14). On the other hand, if we implement it using (38) we will denote it as Markov ORD (M-ORD), since in addition to the Gaussian assumption we use the first order Markov assumption in the ratio sequence z.

4. Performance evaluation: analytical

The decision rule for the Optimum Ratio Detector (ORD), has a quadratic form given in (32) of Section 3.2. A more concise expression for (32) is achieved:

$$(\mathbf{z}''-\mathbf{s})^T\mathbf{H}(\mathbf{z}''-\mathbf{s}) \gtrless_{-1}^{1} T_1' \tag{39}$$

where we have defined $\mathbf{H} = \mathbf{C}_{|-\mathbf{1}}{}^{-1} - \mathbf{C}_{|\mathbf{1}}{}^{-1}$, $\mathbf{k} = \mathbf{C}_{|-\mathbf{1}}{}^{-1}\mu_{\mathbf{z}''_{|-\mathbf{1}}} - \mathbf{C}_{|\mathbf{1}}{}^{-1}\mu_{\mathbf{z}''_{|\mathbf{1}}}$, $\mathbf{s} = \mathbf{H}^{-\mathbf{1}}\mathbf{k}$, $T_1' = T_1 + \mathbf{s}^T\mathbf{H}\mathbf{s}$, and where $\mathbf{s}^T\mathbf{H}\mathbf{s}$ is added for completing the square.

The symmetric matrix $\mathbf{C}$ admits eigendecomposition as $\mathbf{C} = \mathbf{U}\,\mathrm{diag}(\lambda_i)\mathbf{U}^T$, where $\mathbf{U}$ is the modal matrix of eigenvectors and λ_i are the eigenvalues. Thus, using (30) the eigendecompositions of $\mathbf{C}_{|\delta}$ for $\delta\in\{-1,1\}$ embedding can be written as $\mathbf{C}_{|\delta} = \mathbf{U}\,\mathrm{diag}(\lambda_{i|\delta}+\sigma_\zeta^2)\mathbf{U}^T$, where $\lambda_{i|\delta} = \alpha^{2\delta}\lambda_i$. Therefore, $\mathbf{H} = \mathbf{C}_{|-\mathbf{1}}{}^{-1} - \mathbf{C}_{|\mathbf{1}}{}^{-1}$ can be shown as:

$$\mathbf{H} = \mathbf{U}\,\mathrm{diag}\left(\frac{1}{\lambda_{i|-1}+\sigma_\zeta^2}-\frac{1}{\lambda_{i|1}+\sigma_\zeta^2}\right)\mathbf{U}^T \tag{40}$$

Substituting (40) in (39), we have:

$$(\mathbf{z}''-\mathbf{s})^T\mathbf{U}\,\mathrm{diag}\left(\frac{\lambda_{i|1}-\lambda_{i|-1}}{(\lambda_{i|-1}+\sigma_\zeta^2)(\lambda_{i|1}+\sigma_\zeta^2)}\right)\mathbf{U}^T(\mathbf{z}''-\mathbf{s}) \gtrless_{-1}^{1} T_1' \tag{41}$$

If we define $\mathbf{d} = \mathrm{diag}(g_i)\mathbf{U}^T(\mathbf{z}''-\mathbf{s})$, where

$$g_i = \sqrt{[\lambda_{i|1}-\lambda_{i|-1}]/\left[(\lambda_{i|-1}+\sigma_{n_z}^2)(\lambda_{i|1}+\sigma_{n_z}^2)\right]},$$

we can express the detector in terms of its sufficient statistics, D:

$$D = \sum_{i=1}^{\frac{N}{2}} d_i{}^2 \gtrless_{-1}^{1} T_1' \tag{42}$$

The performance can be analytically studied if we can obtain an explicit expression for the distribution of the sufficient statistics, D. The characteristic function of d_i^2 which are squared Gaussian variates is given as $\frac{1}{\sqrt{(1-jw\sigma_{d_i}^2)}}\exp\{-\frac{jw\mu_{d_i}^2}{1-jw\sigma_{d_i}^2}\}$. Moreover, since d_i^2's are independent, the characteristic function of D can be expressed in the product form:

$$\Psi_D(jw) = \prod_{i=1}^{\frac{N}{2}}\frac{1}{\sqrt{(1-jw\sigma_{d_i}^2)}}\exp\left\{-\frac{jw\mu_{d_i}^2}{1-jw\sigma_{d_i}^2}\right\} \tag{43}$$

In this expression, μ_{d_i} represents the mean of d_i, which for $\delta\in\{-1,1\}$ embedding becomes $\mu_{d_i|\delta} = g_i(\mathbf{U}^T(\mu_{\mathbf{z}''_{|\delta}}-\mathbf{s}))_i$.

Similarly, $\sigma_{d_i}^2$, the variance of d_i, can be computed from the covariance matrix of $\mathbf{d}$. Since $\mathbf{s}$ is a constant term, the covariance matrix of $\mathbf{d}$ is given by:

$$\mathrm{Cov}(\mathbf{d}) = \mathbf{U}^T\,\mathrm{Cov}(\mathbf{z}'')\mathbf{U} = \mathbf{U}^T\mathbf{U}\,\mathrm{diag}(\lambda_i'')\mathbf{U}^T\mathbf{U} = \mathrm{diag}(\lambda_i'') \tag{44}$$

Thus, the variance is given as $\sigma_{d_i|\delta}^2 = g_i^2(\lambda_{i|\delta}+\sigma_n^2)$.

The characteristic function of the decision variable, D in (32) is not tractable. However, we can invoke the central limit theorem for suitably large N, and model D as a Gaussian variate. The mean and variance of the Gaussian approximation to D are calculated as:

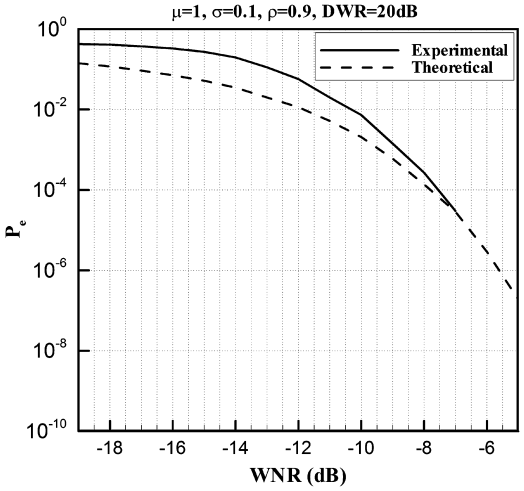

Fig. 5. Comparison between the theoretical error probability and experimental one for a signal with model parameters $[\mu = 1, \sigma = 0.1, \rho = 0.9]$ in DWR = 20 dB.

$$\mu_{D|\delta} = \frac{1}{j}\frac{\partial \Psi_{D|\delta}(jw)}{\partial w}\bigg|_{w=0} = \sum_{i=1}^{\frac{N}{2}} (\sigma^2_{d_i|\delta} + \mu^2_{d_i|\delta}) \tag{45}$$

$$\sigma^2_{D|\delta} = \frac{1}{j^2}\frac{\partial^2 \Psi_{D|\delta}(jw)}{\partial w^2}\bigg|_{w=0} - \mu^2_{D|\delta} = \sum_{i=1}^{\frac{N}{2}} (2\sigma^4_{d_i|\delta} + 4\sigma^2_{d_i|1}\mu^2_{d_i|\delta}). \tag{46}$$

The error probability is given as:

$$P_e = \frac{1}{2}P(D_{|1} < T'_1) + \frac{1}{2}P(D_{|-1} > T'_1) = \frac{1}{2}\left[1 + Q\left(\frac{T'_1 - \mu_{D|-1}}{\sigma_{D|-1}}\right) - Q\left(\frac{T'_1 - \mu_{D|1}}{\sigma_{D|1}}\right)\right] \tag{47}$$

where $Q(x)$ is the complementary error function and is defined as $Q(x) = \frac{1}{\sqrt{2\pi}}\int_x^\infty e^{-\frac{t^2}{2}}\,dt$.

This is the closed form of the error probability of the decoder. In Fig. 5 we compared this theoretical error probability with the experimental case of a signal with model parameters $[\mu = 1, \sigma = 0.1, \rho = 0.9]$ in DWR = 20 dB (DWR will be defined in the next section). As we can see the theoretical and experimental results match perfectly.

5. Performance evaluation: experimental

In this section, we present experimental performance results of our watermarking method under AWGN attack. The strength of the watermarking is expressed in terms of the Document-to-Watermark Ratio (DWR) defined as:

$$\text{DWR} = 10\log_{10}\frac{E\|\mathbf{u}\|^2}{E\|\mathbf{u}' - \mathbf{u}\|^2} \tag{48}$$

where $\mathbf{u}$ is the host signal and $\mathbf{u}'$ is the watermarked signal. As discussed in Section 3.1, for the proposed watermarking methods, we have $x_i = u_{2i-1}$ and $y_i = u_{2i-1}$. Besides, we have $x'_i = u'_{2i-1} = \alpha u_{2i-1} = \alpha x_i$ or $x'_i = u'_{2i-1} = \frac{1}{\alpha}u_{2i-1} = \frac{1}{\alpha}x_i$ respectively for '1' or '−1' embedding and $y'_i = u'_{2i} = u_{2i} = y_i$. Thus, $\mathbf{x}$ and $\mathbf{y}$ will have the same means and variances; therefore $E\|\mathbf{u}\|^2 = E\|\mathbf{x}\|^2 + \|\mathbf{y}\|^2 = 2E\|\mathbf{x}\|^2$, and

$$E\|\mathbf{u}' - \mathbf{u}\|^2 = E\|\mathbf{x}' - \mathbf{x}\|^2 + E\|\mathbf{y}' - \mathbf{y}\|^2 = \frac{1}{2}E\|\alpha\mathbf{x} - \mathbf{x}\|^2 + \frac{1}{2}E\left\|\frac{\mathbf{1}}{\alpha}\mathbf{x} - \mathbf{x}\right\|^2 + 0 = \frac{(\alpha-1)^2 + (\frac{1}{\alpha}-1)^2}{2}E\|\mathbf{x}\|^2$$

Therefore, we can rewrite (48) as:

$$\text{DWR} = -10\log_{10}\frac{(\alpha-1)^2 + (\frac{1}{\alpha}-1)^2}{4} \tag{49}$$

We fix DWR for each experiment and test our methods for different Watermark-to-Noise Ratios (WNR), defined as:

$$\text{WNR} = 10\log_{10}\frac{E\|\mathbf{u}' - \mathbf{u}\|^2}{E\|\mathbf{u}'' - \mathbf{u}'\|^2} \tag{50}$$

where $\mathbf{u}''$ is the received signal. Then, we can rewrite (50) as:

$$\text{WNR} = 10\log_{10}\left[\frac{(\alpha-1)^2 + (\frac{1}{\alpha}-1)^2}{4}\cdot\frac{E\|\mathbf{u}\|^2}{E\|\mathbf{n}\|^2}\right] = 10\log_{10}\left[\frac{(\alpha-1)^2 + (\frac{1}{\alpha}-1)^2}{4}\cdot\frac{\sigma^2 + \mu^2}{\sigma_n^2}\right] \tag{51}$$

5.1. Verification of first-order Markov assumption

In the first experiment, we verify the accuracy of first-order Markov assumption made in Section 3 to simplify the ML decoder as in (38). To this end, we compare the performance of M-ORD and G-ORD for five different settings of the source model parameters, namely, $[\mu = 1, \sigma = 0.1, \rho = 0.9]$, $[\mu = 1, \sigma = 0.15, \rho = 0.8]$, $[\mu = 1, \sigma = 0.2, \rho = 0.7]$, $[\mu = 1, \sigma = 0.25, \rho = 0.6]$, and $[\mu = 1, \sigma = 0.3, \rho = 0.5]$, in three different DWR values of 20 dB, 16 dB, and 14 dB. The results for WNRs in the range of $[-6; 10]$ are given in Fig. 6. As shown in this figure, in different environments and with different signal settings the M-ORD matches perfectly with G-ORD, which confirms the validity of the Markov assumption. In the latter experiments, we use M-ORD as the default version of the proposed algorithm. We can also see that for all situations our decoder is quite robust even in high noise conditions resulting in low WNR values.

5.2. Input sequence length

Next, we investigate the impact of N, the length of input sequence $\mathbf{u}$, on the performance of the proposed decoder. Here, we tested the performance for signal with parameters $[\mu = 1, \sigma = 0.1, \rho = 0.9]$ in three DWRs of 25 dB, 20 dB, and 16 dB, while we fixed the WNR to 0 dB. The results for N varying between 4 and 100 is shown Fig. 7A. As expected by increasing N the robustness increases. But, we can observe that even for very small sequences we have high robustness. This behavior demonstrates the effectiveness of the proposed algorithm as in real applications we may have signals of small length.

5.3. Parameter estimation

Next, we investigate the dependency of the system to the parameter estimations. Fig. 8 compares the detection performances with parameters estimated from the received sequences and with the ground truth parameters for different signal settings. As we see the performance of results obtained with estimated parameters highly agree with those with ground truth parameters. Also, we can observe that for larger input sequence length N the gap between the results of estimated and ground-truth parameters slightly decreases.

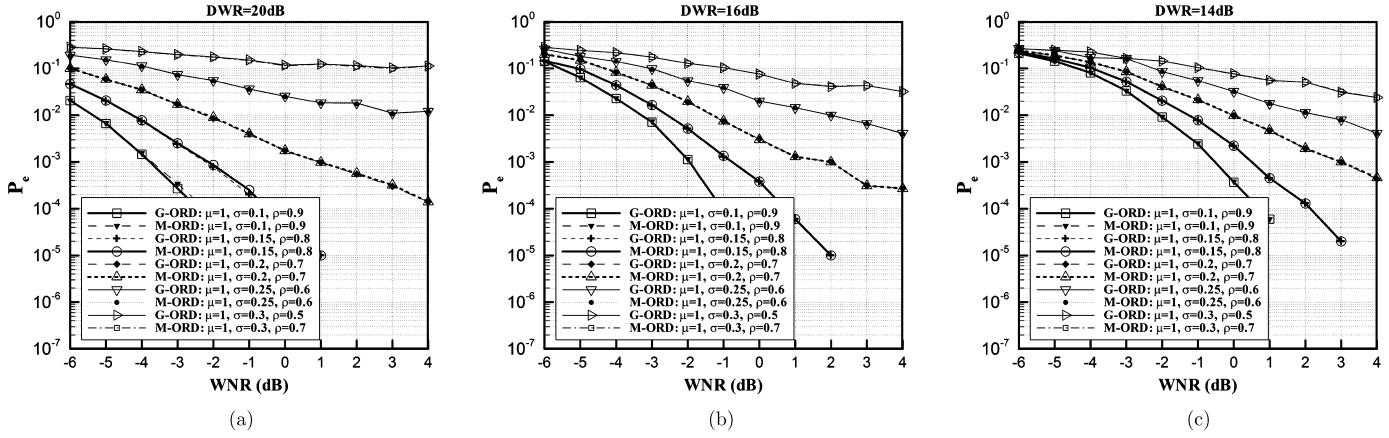

Fig. 6. Probability of error of the ORD decoder for five parameter settings 1) $[\mu = 1, \sigma = 0.1, \rho = 0.9]$, 2) $[\mu = 1, \sigma = 0.15, \rho = 0.8]$, 3) $[\mu = 1, \sigma = 0.2, \rho = 0.7]$, 4) $[\mu = 1, \sigma = 0.25, \rho = 0.6]$, 5) $[\mu = 1, \sigma = 0.3, \rho = 0.5]$, (a) DWR = 20 dB, (b) DWR = 16 dB, (c) DWR = 14 dB.

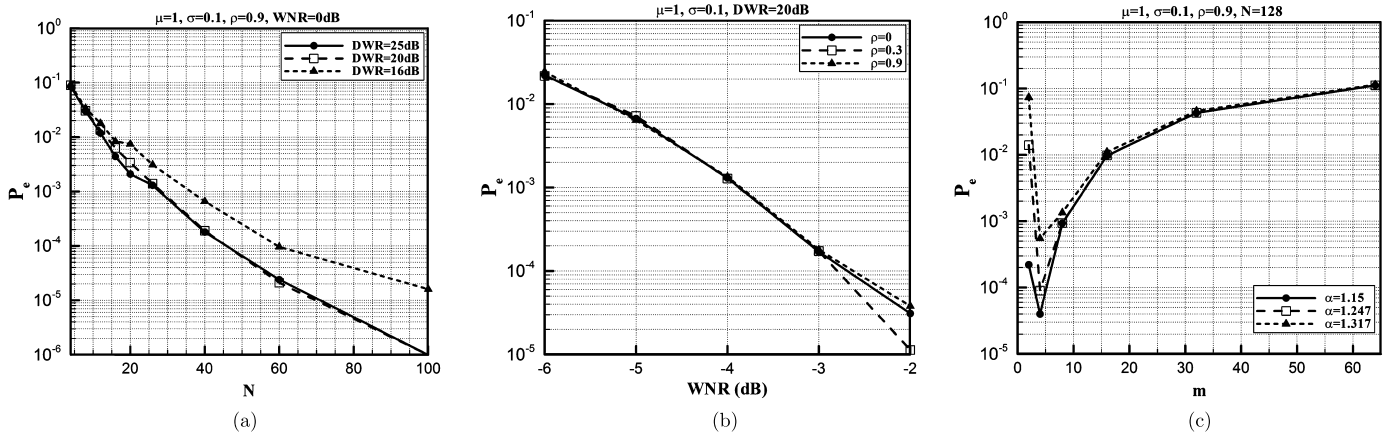

Fig. 7. (a) Effect of changing N, the length of input sequence $\mathbf{u}$ on the performance of the proposed algorithm for a test case of $\mu = 1$, $\sigma = 0.1$, $\rho = 0.9$ in WNR = 0 dB. (b) Performance using the random splitting of the samples for watermarking purpose. Result are given in DWR = 20 dB for three host signals all with the same means and variances $[\mu = 1, \sigma = 0.1]$, but with three different correlation coefficients $\rho = 0, 0.1,$ and 0.9. (c) Effect of changing m, the proportion of untouched/watermarked samples. Results are given for three watermarking strength $\alpha = 1.15, 1, 247,$ and 1.317. The input sequence $\mathbf{u}$ is of length 128 and has the parameter setting of $\mu = 1$, $\sigma = 0.1$, $\rho = 0.9$.

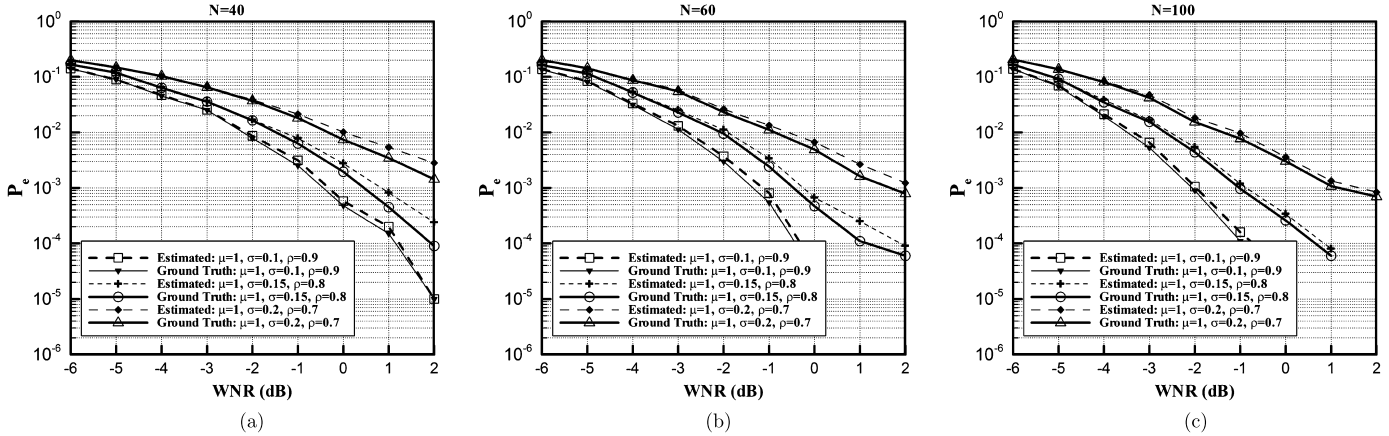

Fig. 8. Comparing the detection performances with parameters estimated from the received sequences and with the ground truth parameters for three parameter settings 1) $[\mu = 1, \sigma = 0.1, \rho = 0.9]$, 2) $[\mu = 1, \sigma = 0.15, \rho = 0.8]$, 3) $[\mu = 1, \sigma = 0.2, \rho = 0.7]$, (a) $N = 40$, (b) $N = 60$, (c) $N = 100$.

5.4. Sensitivity to parameter estimation

Next, we explore the sensitivity of the proposed algorithm to the parameter estimation errors. To this aim we deliberately multiple Gaussian noise to the parameters estimated in (33). Performance of the detector in the presence of additive Gaussian noise contamination to the estimated parameters $\hat{\mu}$, $\hat{\sigma}$, and $\hat{\rho}$ is illustrated in Fig. 9. In this figure, the abscissa denotes the standard deviation ν of the multiplicative noise of mean one. We can observe that the ORD scheme is quite robust to the parameter estimation noise.

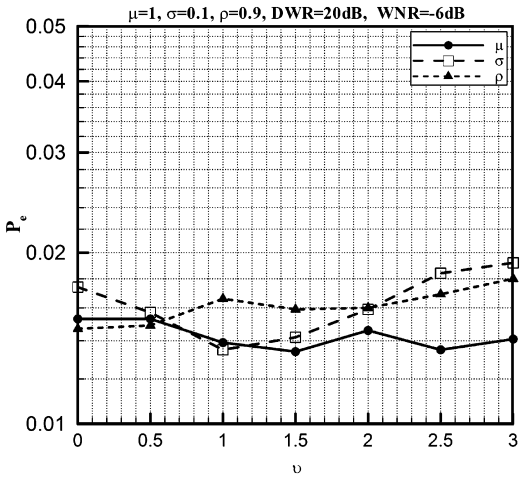

Fig. 9. Sensitivity of ORD scheme to the parameter estimation error. Results are given for distortions in estimation of μ, σ, and ρ with multiplicative noise of $\mathcal{N}(1, v^2)$. The input sequence $\mathbf{u}$ is of length 100 and has the parameter setting of $\mu = 1$, $\sigma = 0.1$, $\rho = 0.9$.

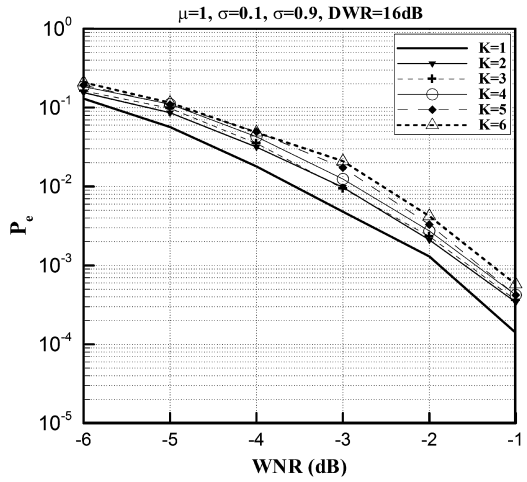

Fig. 10. Performance using multi-bit embedding per block. Result for embedding $K = 1$ to 6 bits-per-block are given in DWR = 16 dB for a host signal of $[\mu = 1, \sigma = 0.1, \rho = 0.9]$ and length $N = 128$.

5.5. Random splitting

To increase the reliability of the model estimation, we consider secure random splitting instead of odd-even splitting of watermarked samples. Thus, half of the randomly selected samples of $\mathbf{u}$ are used for watermarking and the rest of samples for detection purpose. With known indices, the exact decoder can be derived as in Section 3. However, the derivation of a closed form solution is not straightforward. Since scrambling considerably reduces the correlation across the samples, we simplify the decoder using the i.i.d. assumption and replace $\rho = 0$ in (38). In Fig. 7B, we tested the performance for three host signals of length $N = 100$, with the same means and variances as $[\mu = 1, \sigma = 0.1]$ and three different choices of correlation coefficient $[\rho = 0, \rho = 0.3, \rho = 0.9]$ while the DWR was 20 dB in each case. The results indicate that the i.i.d. assumption has a minor effect on the performance of correlated signals and that the scrambled watermarking can preserve its robustness while at the same time increasing the security.

5.6. Proportion of untouched/watermarked samples

We also investigated the impact of the proportion of untouched/watermarked samples. In this experiment, for a signal of length 128 and parameters $[\mu = 1, \sigma = 0.1, \rho = 0.9]$, we tested the performance of the decoder by embedding the watermark in every other m samples. In this case, the ratio sequence $\mathbf{z}$ is defined as

$$z_i = \frac{u_{(i-1)m+1}}{\frac{1}{m-1}\sum_{j=(i-1)m+2}^{im} u_j}, \quad i = 1, \cdots, \frac{N}{m}. \tag{52}$$

To simplify the problem, we have used the i.i.d. decoder. Thus, we could implement the decoder in (38) with only slight modifications. The results are given in Fig. 7C for three different strength factors $\alpha = 1.15, 1.247$, and 1.317 for varying proportion of untouched/watermarked samples m of 2, 4, 8, 16, 32, and 64. Here, the parameter setting is $[\mu = 1, \sigma = 0.1, \rho = 0.9]$ and the noise power σ_n is fixed for each test case. Fig. 7C illustrates that with $m = 4$ we can achieve the best performance.

5.7. Multi-bit embedding

In this subsection, we discuss an extension of the proposed scheme where more than one bit is embedded in each block of samples. To this aim, we employ the sequential attenuation & amplification of orthogonal samples.

Consider, we want to embed K bits in each block. We thus generate $M = 2^K$ orthogonal binary vectors (for example using Walsh–Hadamard codes) of length $N/2$. Let's denote these binary sequences as $\mathbf{B}^{(j)}$, for $j = 1, \cdots, N/2$. Then, we embed the jth binary sequence in the watermark bearing subsequence of the host signal, $\mathbf{x}$, as follows:

$$x'_i = \begin{cases} x_i \cdot \alpha & \text{if } \mathbf{B}_i^{(j)} = 1 \\ x_i \cdot \frac{1}{\alpha} & \text{if } \mathbf{B}_i^{(j)} = -1. \end{cases} \tag{53}$$

As before, we keep the remaining proportion of host samples $\mathbf{y}$ intact. In the decoder side, we use the Markov ML decoding scheme as in the 1-bit case. The only difference in this case is that the density function in (35) should now be computed as:

$$f\left(\mathbf{z}''\middle|\mathbf{B}^{(j)}\right) \simeq \frac{e^{-\sum_{i=1}^{N/2} \bar{z}_i''^2 / 2\sigma^2_{z''|\delta_i^{(j)}}}}{(2\pi)^{N/4} \prod_{i=1}^{N/2} \sigma_{z''|\delta_i^{(j)}}} \left[1 + \sum_{i=2}^{N/2} \frac{\rho_{z''_{i,i-1}} \bar{z}_i'' \bar{z}_{i-1}''}{\sigma_{z''|\delta_i^{(j)}} \sigma_{z''|\delta_{i-1}^{(j)}}}\right], \tag{54}$$

where $\delta_i^{(j)} \in \{-1, 1\}$ is the ith bit of the sequence $\mathbf{B}^{(j)}$. The correlation coefficient $\rho_{z''_{i,i-1}}$ can also computed similar to (36) as

$$\rho_{z''_{i,i-1}} = \rho_z \frac{\sigma_{z'|\delta_i^{(j)}} \sigma_{z'|\delta_{i-1}^{(j)}}}{\sigma_{z''|\delta_i^{(j)}} \sigma_{z''|\delta_{i-1}^{(j)}}}. \tag{55}$$

Thus, the ML decision rule is defined as:

$$j^* = \arg\max_j f\left(\mathbf{z}''\middle|\mathbf{B}^{(j)}\right). \tag{56}$$

To verify the performance of this multi-bit extension of the M-ORD watermarking scheme, we conduct a test on a host signal of length $N = 128$ with parameters $[\mu = 1, \sigma = 0.1, \rho = 0.9]$ on different bits-per-block rates K in DWR = 16 dB. Results illustrated in Fig. 10 reveal that in the multi-bit extension of the proposed scheme the performance degrades gracefully with increasing bit rate. For example, at WNR $= -2$ dB, the error rate increases from 10^{-3} to 5×10^{-3} as the embedding density increases six-fold, from $K = 1$ to $K = 6$.

5.8. Gain attack

As the next experiment, we want to verify the robustness against the gain attack. To this aim, we multiply the samples of

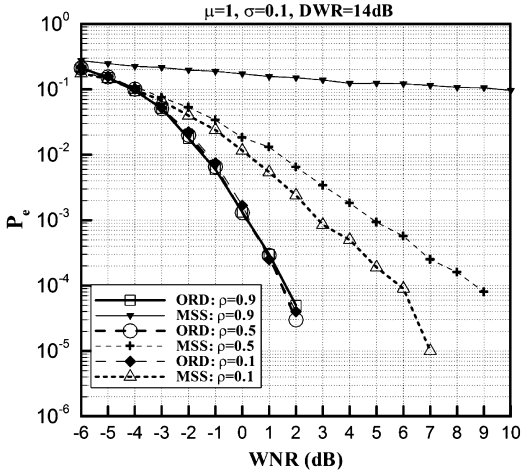

Fig. 11. Comparison between the proposed ORD watermarking method and MSS on host signals of DWR = 14 dB, length $N = 50$, $\mu = 1$, $\sigma = 0.1$, for various correlation coefficients of $\rho = 0.9, 0.5, 0.1$.

the watermarked signal $\mathbf{u}'$ with a variable gain signal $\mathcal{G}$ of sine shape with variable amplitude:

$$\mathcal{G}_i = 1 + M \sin\left(2\pi f \frac{i}{N}\right), \tag{57}$$

where N is the length of the sequence, N is the amplitude and f is the frequency. Thus, the attacked signal will be $u_i'' = u_i' \mathcal{G}_i$. This attack is an intense attack and can destroy the watermark to large extent. However, our algorithm shows perfect robustness with $BER = 0$ for f ranging in $[0, N/8]$ and $M < 0.7$. Therefore, besides the invariance to the constant gain attack (corresponding to $f = 0$), the proposed watermarking scheme shows high robustness to intense variable gain attack as well, which is a remarkable characteristic of the ORD algorithm.

5.9. Comparison

Finally, we compare the ORD scheme against three well-studied spread spectrum watermarking schemes: Multiplicative Spread Spectrum (MSS) [27–30], Improved Spread Spectrum (ISS) [30], and Improved Multiplicative Spread Spectrum (IMSS) [32]

In the first experiment, we compare the proposed scheme and MSS against AWGN attack for the host signal of DWR = 14 dB. Results for different correlation coefficients and fixed mean and variance are shown in Fig. 11. We notice that ORD provides significantly higher robustness as compared to MSS. As expected this performance superiority becomes more prominent for increasingly correlated signals since ORD was designed specifically for such environments.

In the second test, we compare the proposed approach against the Improved Spread Spectrum (ISS) [30] scheme. We test the robustness of ORD and ISS against different strength of the combined AWGN and gain attacks. More specifically we attack the watermarked signal $\mathbf{u}'$ as $u_i'' = \mathcal{G}_i \cdot (u_i' + n_i')$, where $\mathcal{G}$ is the variable gain signal, given as $\mathcal{G}_i = 1 + \mathcal{A} \frac{i}{N} \sin(8\pi \frac{i}{N})$. We test both algorithms on the host signal of DWR = 20 dB, length $N = 32$, and parameters $\mu = 1$, $\sigma = 0.1$, with the sine amplitude $\mathcal{A}$ value is chosen from $\{1/4, 2/4, 3/4\}$, and the correlation coefficient ρ is chosen as 0.1 or 0.9. Result are shown in Table 2. We notice that ORD outperforms ISS specially for higher WNRs. Also, we can note that on more variable gain factors (larger $\mathcal{A}$ values), the superiority of ORD over ISS is more significant, which reveals its higher robustness against the variability of the gain factor.

Finally, we compared the performance of ORD against IMSS [32] technique on a set of 1000 512×512 random test images from BOWS2 database [33] in the embedding rate of 4096 bits. In this experiment, we embed the watermark data in the second level approximation coefficients of the 2-D DWT of each image block using the scaling based technique discussed in Section 3.1 (i.e. the host signal $\mathbf{u}$ is the wavelet coefficients in the second approximation level). We use the Daubechies length-8 Symlet filters with two levels of decomposition to compute the 2-D DWT. Average BER for AWGN and JPEG results are compared in Fig. 12. We can see that ORD has higher robustness than IMSS. The distortion used to watermark the test images using ORD is on average 37 dB.

Table 2
Comparison between the proposed ORD watermarking method and ISS [30] on host signals of DWR = 20 dB, length $N = 32$, and parameters $\mu = 1$, $\sigma = 0.1$, for various correlation coefficients ρ and different sine amplitude values $\mathcal{A}$.

ρ	A	Method	WNR				
			0	1	2	3	4
$\rho = 0.1$	1/4	ORD	5.44	3.95	2.80	1.84	1.21
		ISS	5.56	5.27	5.34	5.47	5.17
	2/4	ORD	1.01	0.36	0.17	0.06	0.02
		ISS	1.37	1.12	0.85	0.94	1.04
	3/4	ORD	0.32	0.100	0.018	0.008	0.001
		ISS	0.064	0.038	0.043	0.020	0.016
$\rho = 0.9$	1/4	ORD	5.08	3.18	2.16	1.30	0.83
		ISS	5.03	5.11	4.81	4.79	4.81
	2/4	ORD	0.74	0.36	0.14	0.05	0.01
		ISS	1.07	1.02	0.83	0.70	0.79
	3/4	ORD	0.192	0.068	0.014	0.002	0.001
		ISS	0.035	0.021	0.016	0.011	0.006

6. Conclusion

We have introduced a scaling based watermarking method. The host signal is assumed to be Gaussian with AR model of order one. The blind algorithm splits the data into two subsets, one for watermarking, the other for parameter estimation at the detector. Although for didactic reasons we have selected the even and odd indexed subsequences, in principle the subset selection may be performed according to a secret key. The statistical characteristics of the ratio of the subset samples have been studied analytically and these results are used in designing our watermarking algorithm.

The error probability of the ORD detector in the presence of AWGN is analytically calculated. It has been shown that for a large range of parameter settings reflecting acceptable document-to-watermark ratios, the detector performs very well even at very low watermark-to-noise ratios.

Besides, the power of watermark as a function of scaling parameter is investigated. Therefore, as a future work the trade-off between robustness and distortion can be mathematically solved via optimization techniques. Experimental results show that the proposed scheme is highly robust against AWGN attack. We are trying to make the algorithm robust against de-synchronization attacks by inserting some codes in specific positions and tracking these codes at the decoder side.

Appendix A. The assumed signal model occurs commonly in real images

Here, we want to show that the assumed signal model in Section 2, with low coefficient of variation, occurs commonly in real-world images. We took 1000 random images of size 256×256 from never-compressed image database[1] and obtained their wavelet approximation coefficients at second decomposition level.

[1] http://www.shsu.edu/qxl005/New/Downloads/index.html

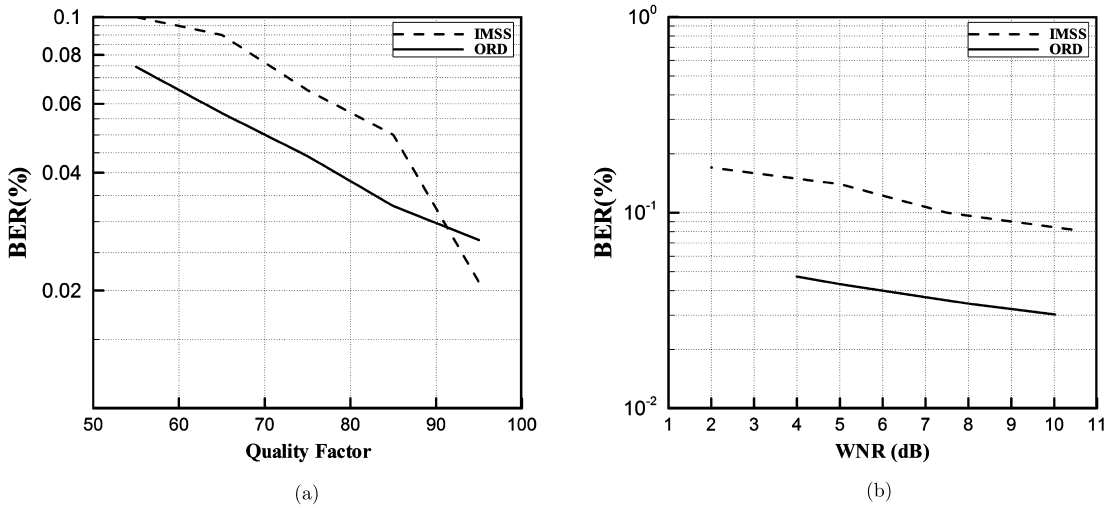

Fig. 12. Comparison between the proposed RSB watermarking method and IMSS [32]: BER (%) under (a) JPEG compression and (b) AWGN attacks.

Then we computed their coefficient of variation, A, their normalized correlation, ρ, and their normalized correlation of the ratio sequence, ρ_z in these bands. Fig. 13 shows their rank-ordered plots; more specifically, we rank ordered the A coefficients (respectively, ρ and ρ_z coefficients) simply for a more regular plot of the spread of these coefficients over arbitrary images. The two important messages to be gleaned from these plots are the following: i) The coefficient of variation A is sufficiently small especially for higher levels of decomposition, which confirms our assumption in Section 2. ii) While the host signal is highly correlated as given in Fig. 13, the correlation of the ratio sequence ρ_z, defined in (12), is small as shown in Fig. 13. Thus for example, we can observe that for the third approximation level we have $A < 0.1$ and $\rho \in [0.1, 0.5]$ which leads us to the KS distance of less than 0.07 in Fig. 1.

To quantitatively evaluate the imperceptibility of the proposed watermark embedding scheme, introduced in Section 3.1, in real applications, we compute the mean structural similarity index (MSSIM) [31] for all 1000 test images, when the watermark data is embedded in their approximation coefficients. MSSIM quality measure is highly matched measure with the human visual system and can effectively capture local errors and artifacts in the spatial domain. Close to one MSSIM values shown in Fig. 13 confirms the imperceptibility of the proposed algorithm.

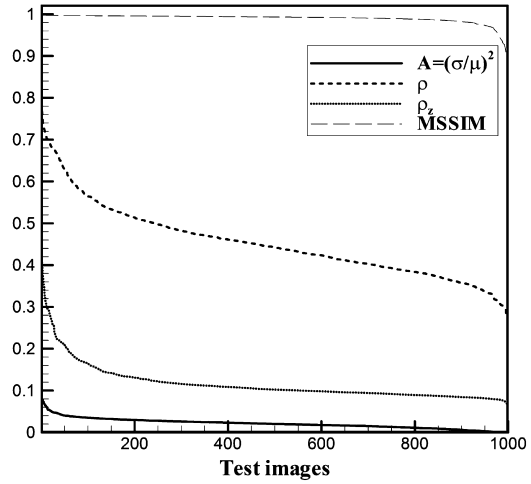

Fig. 13. The coefficient of variation (A), the normalized correlation, ρ, and the normalized correlation of the ratio sequence, ρ_z in the wavelet approximation levels 2, and the MSSIM quality measure for each watermarked image for 1000 test images. (The results are the average values for blocks of size 8×8 in the images of size 256×256 and Images are sorted for better observation.)

Appendix B. Approximating $f(\mathbf{z})$ for $\rho_z \ll 1$

For $\rho_z \ll 1$, we can rewrite (17) as:

$$f(z_2|z_1) \simeq \frac{1}{\sqrt{2\pi\sigma_z^2}} \exp\left\{-\frac{(\bar{z}_2^2 - 2\rho_z \bar{z}_1 \bar{z}_2)}{2\sigma_z^2}\right\} \tag{58}$$

Moreover, for $\rho_z \ll 1$ we can use the tailor series to estimate $e^{\frac{\rho_z \bar{z}_1 \bar{z}_2}{\sigma_z^2}} \simeq 1 + \frac{\rho_z \bar{z}_1 \bar{z}_2}{\sigma_z^2}$. Thus, we have:

$$f(z_2|z_1) \simeq \frac{1}{\sqrt{2\pi\sigma_z^2}} e^{-\frac{\bar{z}_2^2}{2\sigma_z^2}} \left(1 + \frac{\rho_z \bar{z}_1 \bar{z}_2}{\sigma_z^2}\right) \tag{59}$$

Substituting (58) in (16), we have:

$$f(\mathbf{z}) \simeq \frac{e^{-\frac{1}{2\sigma_z^2}\sum_1^{\frac{N}{2}} \bar{z}_i^2}}{\sqrt{(2\pi\sigma_z^2)^{\frac{N}{2}}}} \prod_{i=2}^{\frac{N}{2}} \left(1 + \frac{\rho_z \bar{z}_i \bar{z}_{i-1}}{\sigma_z^2}\right) \tag{60}$$

and by one more step of simplification considering $\rho_z \ll 1$, we have:

$$f(\mathbf{z}) \simeq \frac{e^{-\frac{1}{2\sigma_z^2}\sum_1^{\frac{N}{2}} \bar{z}_i^2}}{\sqrt{(2\pi\sigma_z^2)^{\frac{N}{2}}}} \left[1 + \frac{\rho_z}{\sigma_z^2} \sum_{i=2}^{\frac{N}{2}} (\bar{z}_i \bar{z}_{i-1})\right] \tag{61}$$

References

[1] J. Seitz, Digital Watermarking for Digital Media, Information Science Publishing (2005).
[2] C.S. Lu, Multimedia Security: Stenography and Digital Watermarking Techniques for Protection of Intellectual Property, Idea Group Publishing, 2004.
[3] G.C. Langelaar, I. Setyawan, R.L. Lagendijk, Watermarking digital image and video data: a state-of-the-art overview, IEEE Signal Process. Mag. 17 (5) (2000) 20–46.
[4] I.J. Cox, M.L. Miller, A.L. McKellips, Watermarking as communications with side information, Proc. IEEE 87 (7) (1999) 1127–1141.
[5] S. Katzenbeisser, F.A.P. Petitcolas, Information Hiding Techniques for Steganography and Digital Watermarking, Artech House, Boston, 2000.
[6] M. Barni, F. Bartolini, A. De Rosa, A. Piva, A new decoder for the optimum recovery of nonadditive watermarks, IEEE Trans. Image Process. 10 (5) (2001) 755–766.

[7] M.A. Akhaee, S.M.E. Sahraeian, B. Sankur, F. Marvasti, Robust scaling-based image watermarking using maximum-likelihood decoder with optimum strength factor, IEEE Trans. Multimed. 11 (5) (Aug. 2009) 822–833.
[8] C.T. Hsu, J.L. Wu, Multiresolution watermarking for digital images, IEEE Trans. Circuits Syst. 45 (8) (1998) 1097–1101.
[9] D. Kundur, D. Hatzinakos, Towards robust logo watermarking using multiresolution image fusion principles, IEEE Trans. Image Process. 6 (1) (2004) 185–198.
[10] M. Barni, F. Bartolini, Watermarking Systems Engineering: Enabling Digital Assets Security and Other Applications, CRC, 2004.
[11] Q. Cheng, T.S. Huang, Robust optimum detection of transform domain multiplicative watermarks, IEEE Trans. Signal Process. 51 (4) (2003) 906–924.
[12] T. Ng, H. Garg, Maximum likelihood detection in image watermarking using generalized gamma model, in: Proc. of The 39th Asilomar Conference on Signals, Systems and Computer, CA, USA, 2005, pp. 1680–1684.
[13] V. Solachidis, I. Pitas, Optimal detector for multiplicative watermarks embedded in the DFT domain of non-white signals, EURASIP J. Appl. Signal Process. 24 (16) (2004) 2522–2532.
[14] J. Wang, G. Liu, Y. Dai, J. Sun, Locally optimum detection for Barni's multiplicative watermarking in DWT domain, Signal Process. 88 (2008) 117–130.
[15] M.A. Akhaee, S.M.E. Sahraeian, F. Marvasti, Robust scaling-based image watermarking using maximum-likelihood decoder with optimum strength factor, IEEE Trans. Image Process. 19 (4) (Aug. 2010) 667–680.
[16] N. Khademi-Kalantari, S.M. Ahadi, M. Vafaoost, A robust image watermarking in the ridgelet domain using universally optimum decoder, IEEE Trans. Circuits Syst. Video Technol. 20 (3) (Mar. 2010) 396–406.
[17] J. Liu, P. Moulin, Analysis of interscale and intrascale dependencies between image wavelet coefficients, in: Proc. IEEE Int. Conf. Image Processing (ICIP), Vancouver, Canada, vol. 1, Oct. 2000, pp. 669–672.
[18] T. Pevny, J. Fridrich, Merging Markov and DCT features for multi-class JPEG steganalysis, in: Electronic Imaging, Security, Steganography, and Watermarking of Multimedia Contents IX, San Jose, CA, in: Proc. SPIE, vol. 6505, 2007, pp. 301–314.
[19] W.A. Pearlman, P. Jakatdar, M.M. Leung, Adaptive transform tree coding of images, IEEE J. Sel. Areas Commun. 10 (5) (June 1992) 902–912.
[20] W.A. Pearlman, Adaptive cosine transform image coding with constant block distortion, IEEE Trans. Commun. 38 (5) (May 1990) 698–703.
[21] M. Iwahashi, M. Ohnishi, Analytical evaluation of integerb DCT, in: Proc. Int. Symp. Communication and Information Technology (ISCIT), Sopporo, Japan, 2004.
[22] H.-W. Hsu, C.-M. Liu, Autoregressive modeling of temporal/spectral envelope with finite-length discrete trigonometric transform, IEEE Trans. Signal Process. 58 (7) (July 2010) 3692–3705.
[23] I.K. Yeo, H.J. Kim, Modified patchwork algorithm: a novel audio watermarking scheme, IEEE Trans. Speech Audio Process. 11 (4) (Jul. 2003) 381–386.
[24] A. Papoulis, Probability, Random Variables and Stochastic Processes, 4rd edition, McGraw-Hill, 2004.
[25] D.V. Hinkley, On the ratio of two correlated normal random variables, Biometrika 56 (3) (1969) 635–639.
[26] D.L. Donoho, I.M. Johnstone, Ideal spatial adaptation via wavelet shrinkage, Biometrika 81 (1994) 425–455.
[27] M. Barni, F. Bartolini, A.D. Rosa, Advantages and drawbacks of multiplicative spread spectrum watermarking, in: Proc. SPIE, Santa Clara, CA, Jan. 2003, pp. 290–299.
[28] A. Valizadeh, Z.J. Wang, A framework of multiplicative spread spectrum embedding for data hiding: Performance, decoder and signature design, in: Proc. Global Commun. (GLOBECOM), Dec. 2009, pp. 1–6.
[29] J. Zhong, S. Huang, An enhanced multiplicative spread spectrum watermarking scheme, IEEE Trans. Circuits Syst. Video Technol. 16 (12) (Dec. 2006) 1491–1506.
[30] H.S. Malvar, D.A. Florencio, Improved spread spectrum: a new modulation technique for robust watermarking, IEEE Trans. Signal Process. 4 (51) (Apr. 2003) 898–905.
[31] Z. Wang, A.C. Bovik, H.R. Sheikh, E.P. Simoncelli, Image quality assessment: from error visibility to structural similarity, IEEE Trans. Image Process. 13 (Apr 2004) 600–612.
[32] A. Valizadeh, Z.J. Wang, An improved multiplicative spread spectrum embedding scheme for data hiding, IEEE Trans. Inf. Forensics Secur. 7 (4) (Aug 2012) 1127–1143.
[33] The Dataset from the 2nd Bows Contest. (2012, Mar. 26). Available online: http://bows2.ec-lille.fr/.

Sayed Mohammad Ebrahim Sahraeian received his B.S. and M.S. degrees in electrical engineering from Sharif University of Technology, Tehran, Iran, in 2005 and 2008, respectively. He has received his Ph.D. degree in electrical and computer engineering at Texas A&M University, College Station, TX, in 2013. Now, he is a post-doctoral researcher at the University of California, Berkeley, CA. His research interests include image and multidimensional signal processing, genomic signal processing, bioinformatics, and computational biology.

Mohammad Ali Akhaee received his B.Sc. degree in both electronics and communications engineering from Amirkabir University of Technology, and the M.Sc. and Ph.D. degree in communication systems from Sharif University of Technology in 2005 and 2009, respectively. He has awarded governmental Endeavour research fellowship from Australia in 2010. He is an author/coauthor of more than 40 papers and holds one Iranian patent. He served as the technical program chair of EUSIPCO'11.

Dr. Akhaee serves as a faculty member at the College of Eng., University of Tehran, Tehran, Iran. His research interests include multimedia security, cryptography, watermarking, and statistical signal processing.

Blent Sankur has received his B.S. degree in Electrical Engineering at Robert College, Istanbul and completed his M.Sc. and Ph.D. degrees at Rensselaer Polytechnic Institute, New York. He is presently at Bogazii (Bosphorus) University in the Department of Electrical-Electronic Engineering. His research interests are in the areas of digital signal processing, image and video compression, biometry, cognition and multimedia systems. He is the founder and leader of the image and signal processing laboratory at Bogazii, and has been serving in various industrial consulting tasks. Dr. Sankur has held visiting positions at the University of Ottawa, Technical University of Delft, and Ecole Nationale Suprieure des Telecommunications, Paris. He was the chairman of ICT'96: International Conference on Telecommunications and of EUSIPCO'05: The European Conference on Signal Processing, as well as technical chairman of ICASSP'00.

Farokh Marvasti received his B.Sc., M.Sc. and Ph.D. degrees in 1970, 1971 and 1973 respectively, all in electrical engineering from Rensselaer Polytechnic Institute. He was an associate professor of Illinois Institute of Technology during 1987–1991 and from 1992 to 2003 he was an instructor at King's College, London. He was granted several research grants. Currently, he is professor of Sharif University of Technology, Tehran, Iran. His general research interests lie in signal processing, multiple access, MIMO techniques and information theory.